

Multi-element analysis of geological samples using ICP-MS equipped with integrated sample introduction and aerosol dilution systems

NAKAMURA Atsunori^{1*}, KUBOTA Ran¹ and OHTA Atsuyuki¹

NAKAMURA Atsunori, KUBOTA Ran and OHTA Atsuyuki (2023) Multi-element analysis of geological samples using ICP-MS equipped with integrated sample introduction and aerosol dilution systems. *Bulletin of the Geological Survey of Japan*, vol. 74(2), p. 71–85, 4 figs, 9 tables.

Abstract: Advances in inductively coupled plasma mass spectrometry (ICP-MS) have facilitated multi-elemental analyses of various geological samples. However, time-efficient measurement of high-matrix samples is challenging. In this study, we demonstrate the experimental setup of a new ICP-MS, Agilent 7900, equipped with a collision/reaction cell (CRC), an ultra-high matrix introduction (UHMI) system, and a third-generation integrated sample introduction system (ISIS3). The CRC effectively reduces molecular interference. To obtain a sufficiently low background equivalent concentration and blank/standard ratio, the He gas flow rate was set to 4.5 mL/min. The UHMI system is an aerosol dilution system that minimizes the matrix effect, reducing the interference from doubly charged ions, element oxide ions, plasma-based polyatomic ions, acid-based polyatomic ions, and matrix-based polyatomic ions. The ten-fold dilution mode (HMI-8) was very effective in minimizing the formation rate of oxide ions and matrix-based polyatomic ions. For the quantitative multi-element analysis of geochemical samples, the matrix effect caused by the decrease in ionization efficacy owing to coexisting major elements is a severe problem. However, the matrix effect for trace elements has not been successfully corrected using the internal standard method for natural sample measurements. Therefore, we used a matrix-matched standard solution prepared from JB-1a by adding Li, Be, Ni, Cu, Zn, As, Mo, Ag, Cd, Sn, Sb, Cs, Tl, Pb, and Bi. The ISIS3 reduced the measurement time by approximately 80 min when measuring 42 elements in 50 samples compared with the previous sample introduction system, in which the measurement solution was diluted with water. With the optimized setting parameters, we confirmed that the concentrations of 42 elements in the eight geochemical reference materials were comparable to their referenced values.

Keywords: multi-element analysis, time-efficient measurement, high-matrix sample, matrix effect, isobaric molecular interference, spectral interference, doubly charged ion, oxide ion, ICP-MS

1. Introduction

Technical developments in inductively coupled plasma mass spectrometry (ICP-MS) have contributed to advancements in various disciplines of geochemistry. However, measuring a large number of high-matrix samples is still challenging (e.g., Takahashi and Yamada, 2004). Geological Survey of Japan (GSJ), National Institute of Advanced Industrial Science and Technology, has prepared geochemical maps to reveal the natural background of elements on the Earth by measuring 53 elements in 3000 stream and 4900 marine sediment samples (Imai *et al.*, 2004; Imai *et al.*, 2010; Ohta *et al.*, 2021). Currently, we have been conducting high-

resolution geochemical mapping in Kanto region, Chubu region, Kansai region, and Okinawa Islands (Imai *et al.*, 2015; Imai *et al.*, 2019). This requires time-efficient measurements of a large quantity of high-matrix samples (over 2000 samples).

Therefore, we recently introduced a new ICP-MS, Agilent 7900 (Agilent Technologies, Santa Clara, USA), equipped with a collision/reaction cell to lower spectral interference, an integrated sample introduction system to reduce the measurement time, an autosampler to process a large number of samples, and an aerosol dilution system to minimize the matrix effect. However, the degrees of interference and matrix effects when combining highly sensitive Agilent 7900 and the equipped facilities are poorly understood. In this study, we present

¹ AIST, Geological Survey of Japan, Research Institute of Geology and Geoinformation

* Corresponding author: NAKAMURA, A., Central 7, 1-1-1 Higashi, Tsukuba, Ibaraki 305-8567, Japan. Email:nakamura-a@aist.go.jp

the basic performance of the system, highlighting that the interferences and matrix effects are negligible or sufficiently low. The settings described here are applicable to various geological high-matrix samples.

In this study, we first evaluate the performance of a collision/reaction cell (CRC). Second, we demonstrate the performance of the aerosol dilution system, which reduces interferences by doubly charged ions, oxide ions, and isobaric molecular ions. Third, we investigate the matrix effect caused by a decrease in the ionization efficacy of trace elements by coexisting major elements. We then determine the setup parameters of the sample introduction system to improve the time efficiency of the measurements. Finally, we measure 42 elements in geochemical reference materials to evaluate the fundamental performance of our new equipment.

2. Apparatus

An Agilent 7900 mass spectrometer was equipped with standard devices, including a glass nebulizer, a quartz spray chamber cooled at 2°C using a Peltier cooling system, standard nickel sampling and skimmer cones, a quartz torch with 2.5 mm injector, x-lens, and a fourth-generation octopole reaction system (ORS⁴) collision/reaction cell. The ORS⁴ provides fast cell gas switching and the most effective interference removal using kinetic energy discrimination in the He mode (McCurdy *et al.*, 2006). As an optional function, the ICP-MS is equipped with an autosampler (SPS4) for rapid processing of large amounts of sample, a third-generation integrated sample introduction system (ISIS3) for improving the time-efficiency of measurements, and an ultra-high matrix introduction (UHMI) system for high-matrix analysis.

The valve system within the ISIS3 facilitates simultaneous introduction of the solution to the ICP-MS and washing of the tubes that are not used during the measurements (Wilbur and Jones, 2010; Yamanaka and Wilbur, 2014). Therefore, compared with conventional autosampler systems, ISIS3 significantly reduces the time required for sample switching. Figure 1 shows the schematic illustration of the ISIS3. First, the sample solution is rapidly introduced into the sample loop using an ISIS3 piston pump (Fig. 1a). Simultaneously, the carrier solution mixed with the online internal standard solution is nebulized. The carrier solution then passes through the loop as the valve switches, pushing the sample solution into the nebulizer (Fig. 1b). The rinsing of the autosampler probe begins at the same time as the sample is injected, and the measurement begins after the intensity stabilizes. After data acquisition, the valve returns to the load position, the HNO₃ solution pushes out any remaining sample to waste, and the carrier solution rinses the nebulizer (Fig. 1c). Because the unused routes are washed alternately at each stage, the total measurement time can be significantly shortened (Fig. 1d).

The UHMI system employs sample aerosol dilution

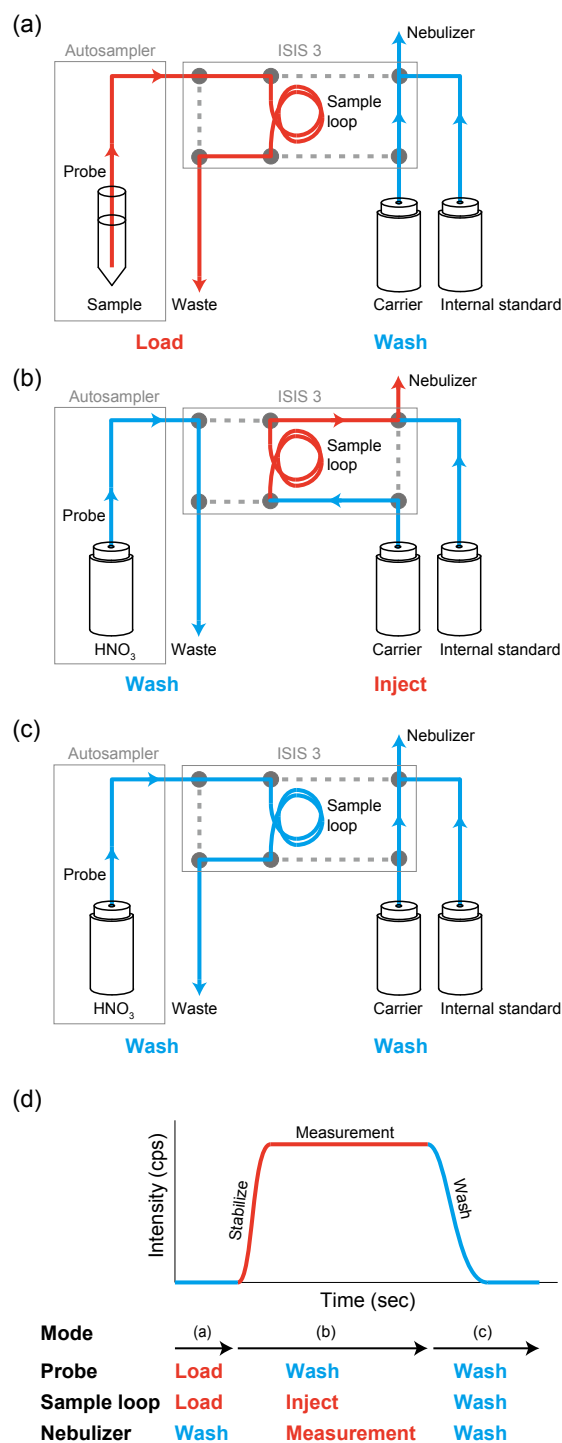


Fig. 1 Schematic illustration of the ISIS3 (modified after Wilbur and Jones, 2010; Yamanaka and Wilbur, 2014): (a) sample loading, (b) sample injection, and (c) sample loop washing. Bold lines in a–c represent active tubes connected by the valves. Dashed lines represent off-line tubes. (d) Change in signal intensity with respect to time. The characters on the arrows indicate the modes of the operation, which are shown in panel a–c. The probe and nebulizer are washed alternately, reducing the total amount of time consumed for a sample.

Table 1 Operating parameters of the ICP-MS.

ICP-MS parameter	No gas mode	He mode
Plasma mode	normal mode	HMI-8
RF power (W)	1,600	
Spray chamber temp (°C)	2	
Sampling depth (mm)	10	
Plasma gas flow (L/min)	15.0	
Carrier gas flow (L/min) ^a	0.95	
Lens tune	Autotune	
Cell gas flow (mL/min)	–	4.5
Stabilization time from No gas mode to He mode (s)	15	
Energy discrimination (V)	5.0	

^aTotal flow rate of nebulizer gas and dilution gas.

technology that uses clean argon gas and is a breakthrough system that eliminates the potential problems of a liquid dilution system. Previously, risks of sample contamination, sample leaks, and dilution errors have been reported for liquid dilution systems (Proper *et al.*, 2020). In contrast, the UHMI system uses a dilution gas, which is introduced through a spray chamber. By diluting with gas rather than water, the UHMI system can significantly reduce the oxide interference. The dilution factor was selected from 1 to 1/100. Herein, the ten-fold dilution mode (HMI-8) was used. The instrumental conditions, including UHMI settings, are summarized in Table 1. The instrumental parameters were set to achieve approximately 1.0 % of the CeO/Ce rate and approximately 1.5 % of the Ce⁺⁺/Ce rate.

3. Experiments

3.1 Reagents

A multi-element calibration solution and an In solution as an internal standard were prepared from a 1000 mg/L atomic absorption standard solution supplied by Kanto Chemical Co., Inc. Briefly, 10000 mg/L or 1000 mg/L ICP-MS standard solutions of Na, Mg, Al, K, Ca, and Fe, supplied by Merck Millipore, were used to evaluate the matrix effect on the declining intensity of minor elements. All acids, including HF, HNO₃, HCl, and HClO₄, were of atomic absorption standard grade supplied by Kanto Chemical Co., Inc. Double-deionized water was produced by RFD300NC (ADVANTEC Co., Inc.) and further purified to 18.2 MΩ resistivity by Milli-Q Simplicity (Merck Millipore). Geochemical reference materials supplied by the Geological Survey of Japan (e.g. Imai *et al.*, 1995; Imai *et al.*, 1996; Terashima *et al.*, 2002; Okai, 2016; Nakamura *et al.*, 2020) were used.

3.2 Optimization of the He gas flow rate in the collision cell

Molecular interference arising from the matrix in the sample solution and Ar gas is reduced by He interactions in the collision cell. Given that the enhanced He gas flow

rate reduces both polyatomic interference and analyte ions, we optimized the cell gas flow rate. The He gas flow rate was increased from 0.0 mL/min to 8.0 mL/min in steps of 0.5 mL/min. To evaluate the interference from ⁴⁰Ar¹⁶O and ⁴⁰Ar³⁸Ar, we measured the ion intensities of ⁵⁶Fe and ⁷⁸Se. For this experiment, a standard solution containing 10 ng/mL Fe and Se was prepared.

The difference in intensity between the standard and the blank is expressed as follows:

$$\Delta I/I = (I_{\text{standard}} - I_{\text{blank}})/I_{\text{standard}},$$

where I_{standard} and I_{blank} are the intensities of the standard and blank solutions, respectively.

3.3 Interference of doubly charged (M⁺⁺) and oxide (MO) ions on analytes

The interference caused by the doubly charged ions and element oxide ions in our system was quantified using 32 elements (Ca, Sc, V, Mn, Fe, Co, Ti, Cr, Ni, Ga, Ge, Se, Zr, Nb, Mo, Sn, Sb, Ba, La, Ce, Pr, Nd, Sm, Eu, Gd, Tb, Dy, Ho, Er, Tm, Yb, and Lu). In particular, we examined the effectiveness of the UHMI system in reducing the interference from the doubly charged ions and element oxide ions. Table 2 shows the measured elements with their masses, the interfered elements with their masses, and the formation rates of the doubly charged and oxide ions. The 32 elements were separated into 15 solutions to avoid overlapping of the doubly charged and oxide ions on the measured masses. Sample solutions containing 10 µg/L and 100 µg/L analytes were measured in normal (without dilution) and in ten-fold dilution modes (HMI-8), respectively.

3.4 Interference of isobaric molecular ions on analytes

Five sample solutions were prepared to evaluate the polyatomic interferences derived from the plasma and/or aqueous matrix (Table 3). Interferences from ⁴⁰Ar³⁸Ar, ⁴⁰Ar²³Na, and ³⁵Cl¹⁶O were evaluated for P, V, Cr, Ni, Cu,

Table 2 Formation rates of doubly charged (M⁺⁺) and oxide (MO) ions.

Mass	Element in solution	M ⁺⁺				MO			
		Interfered element	Analyte mass	No- dilution	HMI-8	Interfered element	Analyte mass	No- dilution	HMI-8
44	Ca	Ne	22	0.50%	0.48%	Ni	60	2.7%	n.d.
48	Ca	Mg	24	n.d.	n.d.	Ni, Zn	64	n.d.	n.d.
45	Sc					Ni	61	0.01%	n.d.
51	V					Zn	67	0.01%	n.d.
55	Mn					Ga	71	<0.01%	n.d.
54	Fe	Al	27	0.75%	n.d.	Ge	70	n.d.	n.d.
59	Co					As	75	<0.01%	<0.01%
47	Ti					Cu	63	5.2%	n.d.
49	Ti					Cu	65	0.90%	n.d.
50	Ti	Mg	25	n.d.	n.d.	Zn	66	31%	n.d.
50	Cr	Mg	25	<0.1%	n.d.	Zn	66	4.9%	n.d.
52	Cr	Mg	26	n.d.	n.d.	Zn	68	0.20%	n.d.
53	Cr					Ga	69	n.d.	n.d.
60	Ni	Si	30	n.d.	n.d.	Ge, Se	76	— ^a	— ^a
62	Ni	P	31	0.15%	n.d.	Se	78	0.15%	0.11%
69	Ga					Rb	85	0.22%	0.17%
74	Ge	Cl	37	n.d.	n.d.	Zr	90	n.d.	n.d.
77	Se					Nb	93	n.d.	n.d.
82	Se	K	41	n.d.	n.d.	Mo, Ru	98	n.d.	n.d.
91	Zr					Ag	107	0.16%	0.07%
93	Nb					Ag	109	0.11%	0.03%
95	Mo					Cd	111	<0.01%	<0.01%
117	Sn					Cs	133	0.18%	0.06%
118	Sn	Co	59	0.39%	n.d.	Ba	134	0.12%	<0.01%
120	Sn					Ba	136	n.d.	<0.01%
123	Sb					La	139	<0.01%	<0.01%
130	Ba	Cu	65	5.1%	0.38%	Nd	146	n.d.	n.d.
135	Ba					Eu	151	0.08%	0.01%
136	Ba	Zn	68	4.1%	2.6%	Sm, Gd	152	0.07%	0.05%
137	Ba					Eu	153	0.05%	0.03%
138	Ba	Ga	69	4.1%	2.8%	Sm, Gd	154	<0.01%	<0.01%
139	La					Gd	155	0.23%	0.12%
140	Ce	Zn, Ge	70	0.97%	0.86%	Gd, Dy	156	0.28%	0.12%
142	Ce	Ga	71	0.93%	0.85%	Gd, Dy	158	0.46%	0.30%
141	Pr					Gd	157	0.39%	0.20%
142	Nd	Ga	71	0.79%	0.75%	Gd, Dy	158	0.33%	0.13%
143	Nd					Tb	159	0.40%	0.18%
150	Nd	As	75	0.72%	0.87%	Er	166	0.35%	0.14%

^a Formation rate was not determined because of interference from ⁴⁰Ar/³⁶Ar.

Zn, As, Se, and Mo. In conjunction with this experiment, we examined the effectiveness of the UHMI system, which reduced the interference of isobaric molecular ions. The analytes and interference species are listed in Table 4. Solution 1 (0.35 mol/L HCl) and solution 2 (0.36 mol/L HNO₃) were measured both in the normal and HMI-8 modes. Solutions 3 L, 4 L, and 5 L were measured in the normal mode (without dilution), whereas solutions 3H,

4H, and 5H were measured in the HMI-8 mode (Table 3).

3.5 Matrix effect due to major elements

The decrease in the ionization efficiency of trace elements (Li, Be, Ni, Cu, Zn, Mo, Cd, Sn, Sb, Cs, Pb, Tl, and Bi) caused by coexisting major elements (Na, Mg, Al, K, Ca, and Fe) in the geological samples was examined. Four solutions were prepared for this experiment (Table

Table 2 Continued.

Mass	Element in solution	M ⁺⁺				MO			
		Interfered element	Analyte mass	No- dilution	HMI-8	Interfered element	Analyte mass	No- dilution	HMI-8
147	Sm					Dy	163	0.05%	0.03%
149	Sm					Dy	165	0.04%	0.05%
150	Sm	As	75	0.51%	0.55%	Er	166	0.10%	0.07%
154	Sm	Se	77	0.63%	0.55%	Er, Yb	170	0.08%	0.04%
151	Eu					Er	167	0.01%	<0.01%
153	Eu					Tm	169	0.01%	0.02%
154	Gd	Se	77	0.36%	0.28%	Er, Yb	170	0.10%	0.05%
156	Gd	Se	78	0.30%	0.28%	Yb	172	0.18%	0.06%
157	Gd					Yb	173	0.20%	0.10%
160	Gd	Se	80	0.61%	0.36%	Yb, Lu	176	0.24%	0.13%
159	Tb			n.d.	0.10%	Lu	175	0.10%	0.10%
160	Dy	Se	80	3.1%	1.6%	Yb, Lu	176	0.06%	0.02%
163	Dy					Hf	179	0.16%	0.06%
164	Dy	Se	82	n.d.	n.d.	Hf, Ta	180	n.d.	n.d.
165	Ho					Ta	181	0.13%	0.06%
167	Er					W	183	0.17%	0.08%
170	Er	Rb	85	0.49%	0.46%	W	186	0.15%	0.10%
169	Tm					Re	185	0.06%	0.02%
173	Yb					Os	189	0.01%	<0.01%
174	Yb	Rb, Sr	87	n.d.	n.d.	Os, Pt	190	0.01%	<0.01%
175	Lu					Ir	191	0.23%	0.10%
176	Lu	Sr	88	n.d.	n.d.	Os, Pt	192	1.1%	0.75%

5) and measured in the HMI-8 mode.

The amounts of trace elements contaminated from the major elemental ICP-MS standard solutions (Na, Mg, Al, K, Ca, and Fe) were calculated as follows:

$$C_{\text{standard}} \times (I_{\text{blank with matrix}} - I_{\text{blank without matrix}}) / (I_{\text{standard without matrix}} - I_{\text{blank without matrix}}),$$

where C_{standard} is the concentration of the standard solution, $I_{\text{blank with matrix}}$ and $I_{\text{blank without matrix}}$ are the intensities of the blank solutions with and without matrix elements, respectively, and $I_{\text{standard without matrix}}$ is the intensity of the standard without matrix elements.

3.6 Quantification of 42 elements in the geochemical reference materials

Eight geochemical reference materials used in this study were obtained from the Geological Survey of Japan: JSd-1, JSd-2, JSd-3, JSd-4 (stream sediments), JLk-1 (lake sediment) (Imai *et al.*, 1996), JSO-1 (soil), JMS-1, and JMS-2 (marine sediments) (Terashima *et al.*, 2002). The analytical method followed in this study was described by Ohta (2018b). First, 0.1 g of a geochemical reference material was weighted in a 50 mL PTFE beaker covered with a PTFE watch glass. The sample was then digested using a mixture containing 5 mL of HF (50%), 3 mL

of HNO₃ (60–61%), and 2 mL of HClO₄ (60–62%) at 125°C for 2 h. After that, the temperature of the sample was increased to 145°C, and the sample was kept at this temperature for 1 h. The digested product was dried at 190°C. The residue was dissolved in 5 mL of 7 mol/L HNO₃. The PTFE beaker was kept at 100°C for 15 min. The dissolved solution was diluted to 100 mL in a polyethylene volumetric flask using double deionized water.

A matrix-matched standard solution was prepared using digested JB-1a (Imai, 1990; Imai *et al.*, 1995). Because the sediment samples of interest yielded significantly higher concentrations of some elements than JB-1a, we added adjustment solutions containing Li, Be, Ni, Cu, Zn, As, Mo, Ag, Cd, Sn, Sb, Cs, Tl, Pb, and Bi to the JB-1a standard solution. This elevated the elemental concentration of the JB-1a-based solution to a level sufficient to obtain a calibration line. Calibration lines were provided using the ion counts of the standard and blank solutions. This procedure is very useful for minimizing the matrix effect in multi-element analyses (Imai, 1990; Ohta, 2018a; Ohta *et al.*, 2021). Furthermore, this method is free from contamination by trace elements contained in the single-element AAS or ICP-MS standards for major elements. The geochemical reference material JB-1a is easily decomposed and its reference values are well documented (Imai, 1990; Imai *et al.*, 1995).

Table 3 Concentrations of the blank and high standard solutions for elucidating the formation of isobaric molecular ions.

Analyte	Solution 1	Solution 2	Solution 3H	Solution 3L	Solution 4H	Solution 4L	Solution 5H	Solution 5L
	mg/L	mg/L	mg/L	mg/L	mg/L	mg/L	mg/L	mg/L
Na	-	-	-	-	100	10	100	10
Mg	-	-	-	-	100	10	100	10
K	-	-	-	-	100	10	100	10
Mn	-	-	-	-	10	1	10	1
S	-	-	20	2	-	-	-	-
Acid	mol/L	mol/L	mol/L	mol/L	mol/L	mol/L	mol/L	mol/L
HNO ₃	0.35	-	0.35	0.35	0.35	0.35	-	-
HCl	-	0.36	-	-	-	-	0.36	0.36

Table 4 Intensities of isobaric molecular ions measured in the normal and HMI-8 modes.

Mass	Element	Abundance (%)	Interference	No-dilution cps / mg/L	HMI-8 cps / mg/L
31	P	100	¹⁴ N ¹⁶ O ¹ H, ¹⁵ N ¹⁶ O	48 cps / 0.35M HNO ₃	36 cps / 0.35M HNO ₃
51	V	99.8	³⁵ Cl ¹⁶ O, ³⁷ Cl ¹⁴ N	1106 cps / 0.36M HCl	230 cps / 0.36M HCl
52	Cr	83.8	³⁶ Ar ¹⁶ O	710 cps / 0.35M HNO ₃	368 cps / 0.35M HNO ₃
53	Cr	9.50	³⁶ Ar ¹⁶ O ¹ H	96 cps / 0.35M HNO ₃	54 cps / 0.35M HNO ₃
53	Cr	9.50	³⁷ Cl ¹⁶ O, ³⁷ Cl ¹⁵ N ¹ H	504 cps / 0.36M HCl	128 cps / 0.36M HCl
60	Ni	26.2	²³ Na ³⁷ Cl	192 cps / Na 10 mg/L (in 0.36M HCl)	72 cps / Na 10 mg / L (in 0.36M HCl)
63	Cu	69.2	⁴⁰ Ar ²³ Na	430 cps / Na 10 mg/L (in 0.35M HNO ₃)	76 cps / Na 10 mg/L (in 0.35M HNO ₃)
65	Cu	30.9	⁴⁰ Ar ²⁵ Mg	214 cps / Mg 10 mg/L (in 0.35M HNO ₃)	10 cps / Mg 10 mg/L (in 0.35M HNO ₃)
66	Zn	27.7	⁴⁰ Ar ²⁶ Mg	152 cps / Mg 10 mg/L (in 0.35M HNO ₃)	14 cps / Mg 10 mg/L (in 0.35M HNO ₃)
66	Zn	27.7	³³ S ³³ S, ³² S ³⁴ S	292cps / S 0.2 mg/L	46 cps / S 0.2 mg/L
75	As	100	⁴⁰ Ar ³⁵ Cl	44 cps / 0.36M HCl	24 cps / 0.36M HCl
77	Se	7.63	⁴⁰ Ar ³⁷ Cl	8 cps / 0.36M HCl	14 cps / 0.36M HCl
78	Se	23.8	⁴⁰ Ar ³⁸ Ar	30 cps / 0.35M HNO ₃	32 cps / 0.35M HNO ₃
80	Se	49.6	⁴⁰ Ar ⁴⁰ Ar	30421 cps / 0.35M HNO ₃	33712 cps / 0.35M HNO ₃
90	Zr	51.5	⁵⁵ Mn ³⁵ Cl	2263 cps / Mn 1 mg/L (in 0.36M HCl)	1526 cps / Mn 1mg/L (in 0.36M HCl)
95	Mo	15.8	⁴⁰ Ar ¹⁶ O ³⁹ K	n.d. / K 10 mg/L (in 0.35M HNO ₃)	n.d. / K 10 mg/L (in 0.35M HNO ₃)
95	Mo	15.8	⁴⁰ Ar ⁵⁵ Mn	n.d. / Mn 1 mg/L (in 0.35M HNO ₃)	n.d. / Mn 1 mg/L (in 0.35M HNO ₃)

The blank, standard, and sample solutions were mixed with a 10 µg/L In solution and diluted ten-fold with the UHMI system (HMI-8). The standard solution was subjected to ICP-MS measurements periodically after the corresponding measurements of every five samples to correct the drift in the signal intensity. The solution of the digested geochemical reference material JB-3 was measured every ten samples for quality control of all the elements. Each of the eight geochemical reference samples was measured thrice.

The detection limit (D.L.) and quantification limit (Q.L.) of 42 trace elements were obtained from ten repeated ICP-MS measurements of a blank solution. D.L. and Q.L. were calculated as follows:

$$D.L. = C_{\text{standard}} \times 3S_{\text{blank}} / (I_{\text{standard}} - I_{\text{blank}}),$$

$$Q.L. = C_{\text{standard}} \times 10S_{\text{blank}} / (I_{\text{standard}} - I_{\text{blank}}),$$

where C_{standard} , S_{blank} , I_{standard} , and I_{blank} are the concentration of the JB-1a standard solution, unbiased standard deviation

obtained from the measurements of the blank solution, intensity of the JB-1a standard solution, and intensity of the blank solution, respectively.

4. Results and discussion

4.1 Optimization of a He gas flow rate

To evaluate the interference caused by ⁴⁰Ar¹⁶O and ⁴⁰Ar³⁸Ar, we measured the ion intensities of ⁵⁶Fe and ⁷⁸Se, and the ion intensities of the standard and blank solutions are shown in Figure 2. When the He cell gas flow was increased from 0 mL/min to 8 mL/min, the ion intensity of the standard and blank solutions increased to a maximum value at a flow rate of 1.0 mL/min. This phenomenon is called the ‘collisional focusing effect’ (Douglas and French, 1992; Takahashi and Yamada, 2004; Tanner *et al.*, 2002). Subsequently, the ion intensity values decreased with increasing gas flow rate owing to the interactions in the collision cell.

The optimal He flow rate is defined as the flow rate

Table 5 Concentrations of blank and high standard solutions for elucidating the matrix effect.

	Blank solution without matrix	Blank solution with matrix	High standard solution without matrix	High standard solution with matrix
Major elements		mg/L		mg/L
Na	-	20	-	20
Mg	-	80	-	80
Al	-	150	-	150
K	-	10	-	10
Ca	-	100	-	100
Fe	-	100	-	100
Trace elements			µg/L	µg/L
Li	-	-	40	40
Be	-	-	4	4
Ni	-	-	400	400
Cu	-	-	400	400
Zn	-	-	500	500
Mo	-	-	10	10
Cd	-	-	4	4
Sn	-	-	40	40
Sb	-	-	10	10
Cs	-	-	10	10
Pb	-	-	200	200
Tl	-	-	2	2
Bi	-	-	10	10

that achieves a sufficiently low background equivalent concentration (BEC) and uniform $\Delta I/I$. Figure 2 shows that the BEC for ^{56}Fe and ^{78}Se decreased to approximately 2.0 $\mu\text{g/L}$ at a He gas flow rate of 4.5 mL/min. The ratios between the signal and background levels converged to 0.8 for ^{56}Fe and 0.9 for ^{78}Se at a He gas flow rate of 4.5 mL/min. Based on these results, the optimum flow rate was set to be 4.5 mL/min for the measurements. While the oxide ratio of $^{156}\text{CeO}/^{140}\text{Ce}$ in our system was reduced from 1.0% to 0.3–0.5% at a He flow rate of 4.5 mL/min, no significant reduction in the double-charged ratio of $^{140}\text{Ce}^{++}/^{140}\text{Ce}$ was observed in our system.

4.2 Interference of doubly charged (M^{++}), and oxide (MO) ions

Table 2 shows the formation rates of doubly charged (M^{++}) and oxide (MO) ions. Overall, these rates were sufficiently low for routine measurements of actual sediment samples. The formation rates of doubly charged ions (M^{++}) were mostly less than 1 %, but were not significantly decreased by HMI-8 dilution. The HMI-8 dilution mode effectively decreased the M^{++} ions for $^{130}\text{Ba}^{++}$, $^{136}\text{Ba}^{++}$, and $^{138}\text{Ba}^{++}$ (interfering with ^{65}Cu , ^{68}Zn , and ^{69}Ga).

The formation of oxide (MO) ions was mostly less than 0.5 % in the normal mode (without dilution), and they decreased further in the HMI-8 dilution mode (Table 2). Although the formation rates of $^{44}\text{Ca}^{16}\text{O}$, $^{47}\text{Ti}^{16}\text{O}$, $^{50}\text{Ti}^{16}\text{O}$, and $^{50}\text{Cr}^{16}\text{O}$ were exceptionally in the range of 2.7–31 % for the normal mode, their formation ratios were

undetectable for the HMI-8 dilution mode. The formation ratio of $^{60}\text{Ni}^{16}\text{O}$ was very high (14–15 %), irrespective of the HMI-8 dilution mode, because of the formation of $^{40}\text{Ar}^{36}\text{Ar}$. Therefore, the isotopes of the analytes ^{76}Ge and ^{76}Se should not be used.

4.3 Interference of isobaric molecular ions

The effectiveness of the UHMI system in reducing plasma-, acid-, and matrix-based polyatomic ions is shown in Table 4. The intensity of the polyatomic ions ranged from ~ 10 cps to ~ 1100 cps, except for $^{40}\text{Ar}^{40}\text{Ar}$. Moreover, $^{40}\text{Ar}^{16}\text{O}^{39}\text{K}$ and $^{40}\text{Ar}^{55}\text{Mn}$ were not detected. These low ion intensities were caused by the capability of the He collision cell. The UHMI system effectively reduced the formation of $^{36}\text{Ar}^{16}\text{O}$, $^{36}\text{Ar}^{16}\text{O}^1\text{H}$, $^{40}\text{Ar}^{23}\text{Na}$, $^{40}\text{Ar}^{25}\text{Mg}$, $^{40}\text{Ar}^{26}\text{Mg}$, $^{35}\text{Cl}^{16}\text{O}$, and $^{33}\text{S}^{33}\text{S}$ (or $^{32}\text{S}^{34}\text{S}$) because the concentrations of matrix elements, such as Na, Mg, Cl, and S, in an aerosol were diluted to one-tenth in the HMI-8 dilution mode. In contrast, the formation rates of $^{14}\text{N}^{16}\text{O}^1\text{H}$, $^{15}\text{N}^{16}\text{O}$, $^{40}\text{Ar}^{37}\text{Cl}$, $^{40}\text{Ar}^{38}\text{Ar}$, and $^{40}\text{Ar}^{40}\text{Ar}$ did not change significantly between the no-dilution and HMI-8 dilution modes. These results suggest that the formation rates of acid-based and plasma-based polyatomic ions were not significantly suppressed by HMI-8 dilution.

4.4 Matrix effect due to major elements (Na, Mg, Al, K, Ca, and Fe)

Table 6 shows that the ionization efficiency of trace elements (Li, Be, Ni, Cu, Zn, Mo, Cd, Sn, Sb, Cs, Pb, Tl,

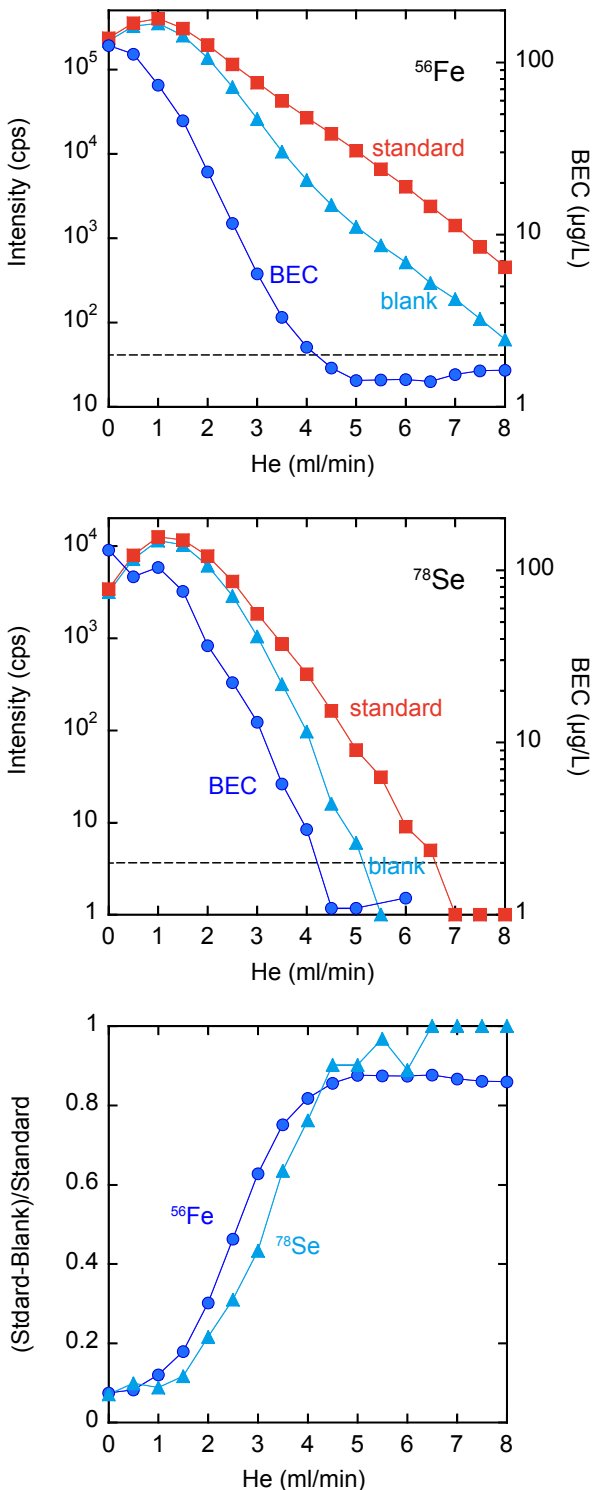


Fig. 2 Optimization of the He gas flow rate. Ion intensities of the standard and blank solutions, BEC, and $\Delta I/I$ are shown.

and Bi) decrease due to coexisting major elements (Na, Mg, Al, K, Ca, and Fe). The amounts of trace elements contaminated from the major elemental ICP-MS standard solutions (Na, Mg, Al, K, Ca, and Fe) are also summarized in Table 6. The lighter isotopes, ⁷Li and ⁹Be, were not affected by matrix elements. In contrast, the intensities of heavier isotopes were significantly reduced by 4–11 % upon adding matrix elements to the solutions.

To overcome the matrix effect, an internal standard solution is often added to standard and blank solutions. In our system, ¹¹⁵In was used as an internal standard to observe the signal drift for a long-time measurement. The decrease in the intensity of the analyte with the major elements was significantly improved by ¹¹⁵In correction (Table 6). The reduction in signal intensity by matrix elements was negligible for ⁹⁵Mo, ¹¹¹Cd, ¹¹⁸Sn, ¹²¹Sb, and ¹³³Cs; however, a significant reduction in the signal intensity was still observed for ⁶⁰Ni, ⁶³Cu, ⁶⁶Zn, ²⁰⁵Tl, ²⁰⁸Pb, and ²⁰⁹Bi. These findings support the advantage of using a matrix-matched calibration solution, which is used for routine measurements. We employed a matrix-matched calibration solution prepared from a geochemical reference material and did not correct the data using ¹¹⁵In.

4.5 Determination of elemental concentrations of measurement samples

4.5.1 Customizing ISIS3 operation for high-matrix samples

Based on results mentioned above, we optimized the operation parameters for the ISIS3 to efficiently measure a large number of samples (Table 7). A loop volume of 2.4 mL is sufficient for a measurement time duration of 200 s. The sample was drawn into a sample loop within the load time. When a sample was injected into the nebulizer, the signal was stabilized in 10 s. After a solution is loaded to the sample loop, the autosampler probe of SPS4 is washed with double deionized water (“Probe rise (MQ)”) and then cleaned by 1 mol/L HNO₃ solution to minimize contamination from a solution (“Probe rise (1 M HNO₃)”). After the measurement, the sample loop was washed with double deionized water (“Optional loop probe wash”) and then cleaned by 1 mol/L HNO₃ solution (“Optional loop wash”).

Previously, we used an Agilent 7500 spectrometer equipped with an ISIS system, which took 230 s to complete a single measurement, including sample load, water dilution, signal stabilization, and washing. In contrast, our new system, Agilent 7900, with the ISIS3, shortened the measurement time to 130 s. Overall, the ISIS3 reduced the total measurement time by approximately 80 min when measuring 42 elements in 50 samples.

These settings were optimized for geological samples with a high matrix. When we measure precious solutions for other studies, we unmount the ISIS3 to minimize the consumption volume of the sample solutions (e.g., Nakamura *et al.*, 2021).

Table 6 Matrix effect of major elements reducing the intensity of trace elements.

Mass	Element	Contamination ($\mu\text{g/L}$) ^a	Intensity declination without In correction	Intensity declination with In correction	Mode
7	Li	0.26	-1.4%	n.d.	No gas
9	Be	0.002	1.3%	n.d.	No gas
60	Ni	0.80	-10%	-7.1%	He
63	Cu	0.31	-11%	-7.6%	He
66	Zn	0.35	-7.5%	-4.2%	He
95	Mo	0.023	-3.7%	-0.3%	He
111	Cd	0.008	-5.0%	-1.7%	He
118	Sn	0.075	-5.5%	-2.2%	He
121	Sb	0.40	-4.8%	-1.4%	He
133	Cs	n.d.	-4.3%	-0.9%	He
205	Tl	0.002	-10%	-6.7%	He
208	Pb	0.050	-11%	-7.8%	He
209	Bi	0.001	-10%	-6.7%	He
115	In		-3.2%	-	He

^a Contamination from ICP-MS standard solution of major elements is calculated.

Table 7 Operating parameters of the ISIS3.

ISIS 3 parameter	Setting
Loop length (mm)	600
Loop tube diameter (mm)	2.18
Loop volume (mL)	2.4

ISIS 3 parameter	Mode ^a	Time (s)
Sample load	(a)	25
Stabilization	(b)	10
Probe rinse (MQ)	(b)	20
Probe rinse (1M HNO ₃)	(b)	20
Optional loop probe wash	(c)	30
Optional loop wash	(c)	25

^a Modes of a, b, and c corresponds to those of Figure 1.

4. 5. 2 Measurement conditions, D. L., and Q. L.

Table 8 summarizes the measurement conditions (analyte, measurement mass, integration time, D.L., and Q.L) of the 42 trace elements. The measurements of ⁷Li and ⁹Be were conducted in the no-gas mode because their intensities were drastically reduced using the He collision mode. The stabilization time from the no-gas mode to the He mode was set to 15 s (Table 1). The intensities of the three masses 206, 207, and 208 were summed to determine the quantity of Pb in the solutions.

4. 5. 3 Determination of elemental concentrations of geochemical reference materials

Figure 3 shows the time-series variation in ion intensities

of ⁷Li, ⁵⁹Co, ⁸⁹Y, ¹¹⁵In, ¹⁴⁰Ce, and ²⁰⁵Tl for the JB-1a standard solution. After 210 min, the ion intensities increased by 1.02–1.09 times compared to the starting values.

Figure 4 shows the time-series variation in ion intensities of ¹¹⁵In for all samples and standards. The intensities of ¹¹⁵In in the samples were higher than that of the JB-1a standard solution and did not increase smoothly with measurement time, indicating the presence of a non-negligible amount of ¹¹⁵In in the samples (Fig. 4). The In concentrations for JSd-3 and JB-1a were reported as 3.9 mg/kg and 0.054 mg/kg, respectively (Terashima, 2001), which result in 3.9 $\mu\text{g/L}$ and 0.054 $\mu\text{g/L}$ of In in solutions, respectively. These solutions were mixed with 10 $\mu\text{g/L}$ In internal solution and then loaded into the nebulizer.

Table 8 Detection limit (D.L.) and quantification limit (Q.L.) calculated from the replicates of the measurement blank solution (n=10).

Mass	Element	Mode	Integration Time (s)	JB-1a	Added high standard	Standard	D.L. (3s)	Q.L. (10s)
				μg/L	μg/L	μg/L	μg/L	μg/L
7	Li	[No Gas]	1	10.9	40	50.9	0.005	0.018
9	Be	[No Gas]	4.5	1.44	4	5.44	0.0002	0.001
45	Sc	[He]	4.5	27.9		27.9	0.020	0.065
51	V	[He]	1.5	205		205	0.016	0.053
52	Cr	[He]	1.5	392		392	0.086	0.287
59	Co	[He]	3	38.6		38.6	0.003	0.011
60	Ni	[He]	3	139	400	539	0.040	0.135
63	Cu	[He]	1.5	56.7	400	457	0.054	0.181
66	Zn	[He]	3	82.1	500	582	0.155	0.517
71	Ga	[He]	3	17.9		17.9	0.005	0.017
75	As	[He]	9	2.3		102	0.056	0.187
85	Rb	[He]	3	39.2		39.2	0.010	0.033
89	Y	[He]	3	24		24	0.001	0.005
90	Zr	[He]	1	144		144	0.009	0.029
93	Nb	[He]	3	26.9		26.9	0.002	0.008
95	Mo	[He]	6	1.57	10	11.6	0.005	0.017
107	Ag	[He]	12	0.041	4	4.04	0.001	0.003
111	Cd	[He]	18	0.1	4	4.1	0.002	0.007
120	Sn	[He]	4.5	2.24	40	42.2	0.049	0.164
121	Sb	[He]	9	0.25	10	10.3	0.002	0.006
133	Cs	[He]	4.5	1.31	10	11.3	0.016	0.052
139	La	[He]	1.8	37.6		37.6	0.003	0.009
140	Ce	[He]	1.5	65.9		65.9	0.002	0.008
141	Pr	[He]	3	7.06		7.06	0.001	0.002
146	Nd	[He]	3	26		26	0.003	0.011
147	Sm	[He]	3	5.07		5.07	0.001	0.003
151	Eu	[He]	3.6	1.46		1.46	0.000	0.001
157	Gd	[He]	3	4.67		4.67	0.001	0.003
159	Tb	[He]	3	0.68		0.68	0.000	0.001
163	Dy	[He]	3	4.06		4.06	0.001	0.002
165	Ho	[He]	3	0.8		0.8	0.0002	0.001
167	Er	[He]	3.6	2.23		2.23	0.001	0.002
169	Tm	[He]	3.6	0.315		0.315	0.0001	0.0005
173	Yb	[He]	3.6	2.05		2.05	0.001	0.003
175	Lu	[He]	4.5	0.305		0.305	0.0001	0.0004
178	Hf	[He]	1.5	3.41		3.41	0.002	0.008
181	Ta	[He]	3.6	1.93		1.93	0.0002	0.001
205	Tl	[He]	6	0.087	2	2.09	0.014	0.047
206	Pb	[He]	3	6.76	200	207	0.014	0.047
207	Pb	[He]	3	6.76	200	207	0.022	0.072
208	Pb	[He]	3	6.76	200	207	0.009	0.029
²⁰⁶⁺²⁰⁷⁺²⁰⁸	Pb ^a			6.76	200	207	0.008	0.026
209	Bi	[He]	7.5	0.016	10	10.0	0.001	0.002
232	Th	[He]	3	9.03		9.03	0.001	0.005
238	U	[He]	3	1.57		1.57	0.0003	0.001
115	In	[No Gas]	0.12			-	-	-
115	In	[He]	0.3			-	-	-

^a Sum of ²⁰⁶Pb, ²⁰⁷Pb, and ²⁰⁸Pb.

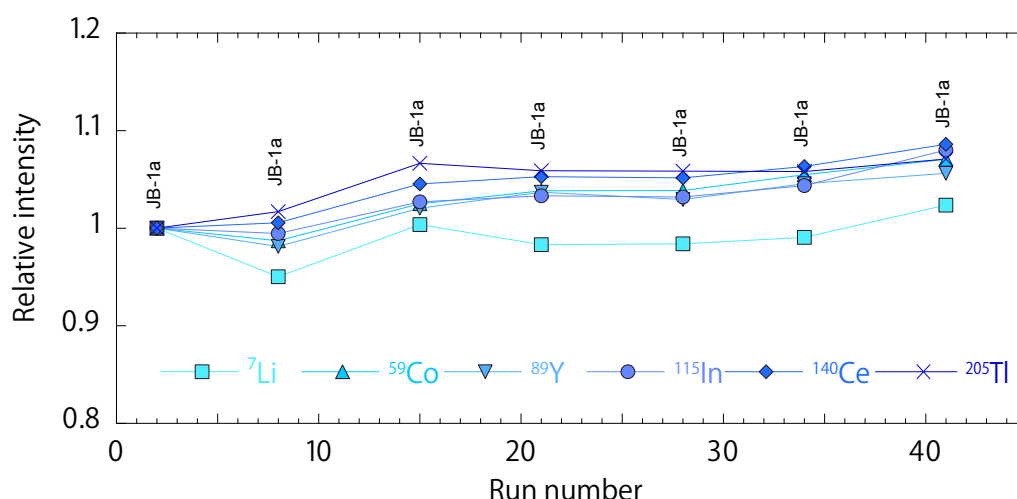


Fig. 3 Changes in signal intensities of ⁷Li, ⁵⁹Co, ⁸⁹Y, ¹¹⁵In, ¹⁴⁰Ce, and ²⁰⁵Tl for the JB-1a standard solution.

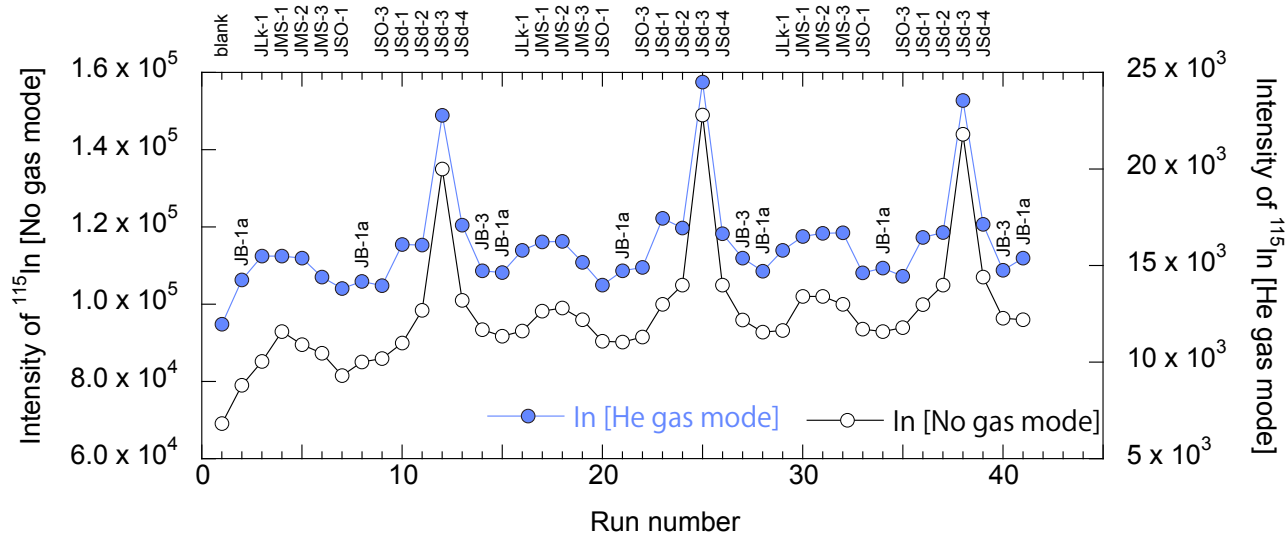


Fig. 4 Changes in signal intensities of ¹¹⁵In (in the He gas and no-gas modes) through three measurement cycles.

Therefore, ¹¹⁵In should not be used as an internal standard without careful consideration of the dilution rate, signal drift, and matrix effect in geological samples.

Overall, the concentrations of 42 elements in the geochemical reference materials were successfully measured and are listed in Table 9. The estimated concentrations and repeatability errors of the elements were comparable to those of the reference values. The coefficients of variation for ⁷Li and ⁹Be were rather high (5–10 %) for JLk-1, JMS-1, JMS-2, and JSO-1; however, those for the other analytes were sufficiently low (less than 5 %). The estimated recovery rates for the samples ranged from 80 % to 110 % of the bulk compositions, with the exception of Zr and Hf. The low recovery rates of Zr and Hf were due to the incomplete decomposition of the heavy

mineral fraction, including zircon.

5. Summary

The experimental setup of the Agilent 7900 mass spectrometer equipped with a CRC, UHMI, and ISIS3 for multi-element analysis of high-matrix samples was demonstrated. The setup was intended to conduct time-efficient measurements for a large number of geological samples. The He gas flow rate of the CRC was set to 4.5 mL/min to sufficiently reduce the molecular interference. The performance of UHMI was examined using the HMI-8 dilution mode and was found to be effective in minimizing the formation rate of oxide ions and matrix-based polyatomic ions. Based on these results,

Table 9 Comparison of analytical data of geochemical reference materials measured using ICP-MS and reference values.

Analyte	JLk-1	JMS-1	JMS-2	JSO-1	JLk-1	JMS-1	JMS-2	JSO-1
	Ave. \pm 1s $\mu\text{g/g}$	Ave. \pm 1s $\mu\text{g/g}$	Ave. \pm 1s $\mu\text{g/g}$	Ave. \pm 1s $\mu\text{g/g}$	ref ^b $\mu\text{g/g}$	ref ^b $\mu\text{g/g}$	ref ^b $\mu\text{g/g}$	ref ^b $\mu\text{g/g}$
7 Li	53.0 \pm 4.0	60.5 \pm 4.5	43.1 \pm 3.4	10.1 \pm 1.1	51.5	62	43	11.2
9 Be	2.89 \pm 0.19	1.51 \pm 0.11	1.95 \pm 0.15	0.64 \pm 0.04	3.31	1.3	1.8	0.69
45 Sc	15.6 \pm 0.5	18.0 \pm 0.4	25.2 \pm 0.8	29.6 \pm 0.6	15.9	-	-	-
51 V	118 \pm 2	128 \pm 3	177 \pm 7	299 \pm 1	117	127	183	300
52 Cr	75.3 \pm 1.3	146 \pm 5	52.8 \pm 1.9	76.7 \pm 1.6	69	133	78	71
59 Co	18.7 \pm 0.2	16.5 \pm 0.5	229 \pm 5	32.2 \pm 0.3	18	18.1	226	32
60 Ni	37.3 \pm 0.3	54.6 \pm 1.5	307 \pm 8	37.5 \pm 0.7	35	53	311	39
63 Cu	65.7 \pm 0.9	89.1 \pm 2.7	451 \pm 9	158 \pm 3	62.9	88	447	169
66 Zn	151 \pm 2	262 \pm 7	160 \pm 5	98.3 \pm 1.5	152	264	166	105
71 Ga	24.2 \pm 0.7	17.6 \pm 0.6	20.4 \pm 0.6	17.1 \pm 0.2	21.4	17.8	17.5	19.3
75 As	18.3 \pm 0.4	17.8 \pm 0.4	36.8 \pm 1.0	6.81 \pm 0.23	26.8	18	35	8.1
85 Rb	151 \pm 2	87.6 \pm 3.5	64.6 \pm 2.5	11.3 \pm 0.2	147	88	65	14.5
89 Y	37.5 \pm 0.3	22.0 \pm 0.6	273 \pm 7	22.6 \pm 0.1	40	24.3	254	24.9
90 Zr	85.9 \pm 2.3	74.6 \pm 1.6	224 \pm 6	74.9 \pm 0.2	137	132	220	96
93 Nb	15.0 \pm 0.1	8.62 \pm 0.24	29.3 \pm 0.8	2.35 \pm 0.05	15.8	9.1	28.1	2.95
95 Mo	1.63 \pm 0.06	2.79 \pm 0.05	23.6 \pm 0.7	0.60 \pm 0.03	1.75	2.7	27.9	-
107 Ag	0.17 \pm 0.01	0.93 \pm 0.03	0.02 \pm 0.01	0.13 \pm 0.01	0.198	-	-	-
111 Cd	0.55 \pm 0.02	0.99 \pm 0.03	0.47 \pm 0.01	0.25 \pm 0.01	0.493	0.5	<0.5	-
120 Sn	4.89 \pm 0.19	5.52 \pm 0.09	2.2 \pm 0.08	1.04 \pm 0.09	5.7	6.6	3.4	1.8
121 Sb	1.83 \pm 0.04	1.13 \pm 0.04	4.04 \pm 0.06	0.32 \pm 0.01	1.68	1.4	4.5	0.38
133 Cs	12.6 \pm 0.1	6.20 \pm 0.19	3.16 \pm 0.1	1.51 \pm 0.02	10.9	5.9	3	1.5
139 La	38.6 \pm 0.6	19.8 \pm 0.6	132 \pm 4	9.13 \pm 0.04	40.6	18.77	130.87	8.91
140 Ce	84.4 \pm 0.4	42.4 \pm 1.1	159 \pm 4	20.0 \pm 0.1	87.9	40.47	155.53	19.9
141 Pr	9.36 \pm 0.15	5.00 \pm 0.14	35.5 \pm 1.1	2.93 \pm 0.06	8.53	4.63	34.93	3.04
146 Nd	35.4 \pm 0.4	19.6 \pm 0.5	150 \pm 3	13.4 \pm 0.2	35.7	19.3	152.93	14.44
147 Sm	7.42 \pm 0.12	4.26 \pm 0.1	34.0 \pm 1.6	3.47 \pm 0.04	7.87	4.00	35.18	3.67
151 Eu	1.20 \pm 0.02	0.99 \pm 0.02	8.39 \pm 0.15	1.05 \pm 0.02	1.27	1.05	9.1	1.22
157 Gd	6.72 \pm 0.09	4.01 \pm 0.1	36.9 \pm 1.0	3.70 \pm 0.05	6.02	4.08	37.46	3.91
159 Tb	1.01 \pm 0.02	0.60 \pm 0.02	5.63 \pm 0.17	0.58 \pm 0.01	1.23	0.60	5.76	0.62
163 Dy	6.04 \pm 0.18	3.75 \pm 0.09	35.7 \pm 0.4	3.65 \pm 0.05	6.57	3.64	36.9	4.01
165 Ho	1.18 \pm 0.04	0.71 \pm 0.03	7.46 \pm 0.24	0.73 \pm 0.02	1.06	0.72	7.87	0.82
167 Er	3.44 \pm 0.05	2.05 \pm 0.05	21.6 \pm 0.5	2.14 \pm 0.04	3.59	2.06	22.51	2.34
169 Tm	0.50 \pm 0.01	0.29 \pm 0.01	2.93 \pm 0.04	0.31 \pm 0.02	0.531	0.29	3.22	0.33
173 Yb	3.30 \pm 0.11	1.95 \pm 0.06	18.9 \pm 0.6	2.09 \pm 0.04	3.99	1.84	18.65	2.07
175 Lu	0.47 \pm 0.01	0.28 \pm 0.01	2.93 \pm 0.14	0.30 \pm 0.01	0.571	0.28	3.14	0.32
178 Hf	2.44 \pm 0.05	1.92 \pm 0.04	4.71 \pm 0.03	1.97 \pm 0.04	3.78	-	15	-
181 Ta	1.43 \pm 0.03	0.77 \pm 0.01	1.81 \pm 0.04	0.19 \pm 0.01	1.57	-	-	-
205 Tl	1.00 \pm 0.02	0.57 \pm 0.013	2.71 \pm 0.04	0.22 \pm 0.01	1.17	-	-	-
Pb ^a	46.9 \pm 0.3	51.4 \pm 1.0	80.6 \pm 1.4	16.2 \pm 0.2	43.7	49	88	13
209 Bi	1.24 \pm 0.02	0.97 \pm 0.03	1.24 \pm 0.03	0.18 \pm 0.01	1.2	1	1.33	0.22
232 Th	18.8 \pm 0.1	7.36 \pm 0.13	13.6 \pm 0.2	1.82 \pm 0.01	19.5	9.2	14.5	3
238 U	3.61 \pm 0.05	2.48 \pm 0.02	2.48 \pm 0.03	0.78 \pm 0.02	3.83	4.8	4.3	1.1

^a Sum of ²⁰⁶Pb, ²⁰⁷Pb, and ²⁰⁸Pb.

^b The reference values are from Imai *et al.* (1996), Terashima *et al.* (2002), and the certificate for JSd-4.

Table 9 Continued.

Analyte	JSD-1	JSD-2	JSD-3	JSD-4	JSD-1	JSD-2	JSD-3	JSD-4
	Ave. \pm 1s	Ave. \pm 1s	Ave. \pm 1s	Ave. \pm 1s	ref ^b	ref ^b	ref ^b	ref ^b
	$\mu\text{g/g}$	$\mu\text{g/g}$	$\mu\text{g/g}$	$\mu\text{g/g}$	$\mu\text{g/g}$	$\mu\text{g/g}$	$\mu\text{g/g}$	$\mu\text{g/g}$
7 Li	24.1 \pm 0.7	22.3 \pm 0.3	159 \pm 5	33.2 \pm 0.9	22.8	19.2	151	32
9 Be	1.27 \pm 0.03	0.96 \pm 0.01	10.1 \pm 0.1	1.16 \pm 0.06	1.4	1.04	9.08	-
45 Sc	11.3 \pm 0.6	18.1 \pm 0.3	11.2 \pm 0.3	16.5 \pm 0.1	10.9	17.5	10.5	17
51 V	81.0 \pm 2.8	132 \pm 2	76.4 \pm 1.2	153 \pm 3	76	125	70.4	152
52 Cr	23.0 \pm 1.0	99.1 \pm 1.9	40.4 \pm 1.4	1300 \pm 20	21.5	108	35.3	1215
59 Co	11.5 \pm 0.4	50.3 \pm 1.0	13.1 \pm 0.3	20.4 \pm 0.4	11.2	48.4	12.7	21
60 Ni	7.15 \pm 0.2	95.9 \pm 1.3	19.8 \pm 0.4	108 \pm 2	7.04	92.8	19.6	114
63 Cu	23.4 \pm 0.8	1120 \pm 30	452 \pm 12	485 \pm 9	22	1117	426	486
66 Zn	103 \pm 3	2080 \pm 40	145 \pm 3	1470 \pm 10	96.5	2056	136	1485
71 Ga	16.9 \pm 1.0	13.7 \pm 0.6	13.8 \pm 0.5	14.7 \pm 0.5	17.2	15.3	13.5	-
75 As	1.97 \pm 0.06	27.9 \pm 0.4	264 \pm 6	52.4 \pm 0.7	2.42	38.6	252	-
85 Rb	72.1 \pm 2.4	27.1 \pm 0.5	315 \pm 7	52.6 \pm 0.8	67.4	26.9	285	57
89 Y	15.4 \pm 0.6	16.9 \pm 0.2	11.2 \pm 0.2	19.5 \pm 0.3	14.8	17.4	14.9	21
90 Zr	21.4 \pm 0.8	31.1 \pm 1.8	47 \pm 1.1	81.1 \pm 1.4	132	111	124	90
93 Nb	11.1 \pm 0.5	3.79 \pm 0.04	7.18 \pm 0.12	6.61 \pm 0.19	11.1	4.56	7.8	-
95 Mo	0.48 \pm 0.01	15.8 \pm 0.3	1.62 \pm 0.06	4.84 \pm 0.05	0.45	14.5	1.73	-
107 Ag	0.03 \pm 0.01	0.97 \pm 0.07	2.83 \pm 0.19	3.15 \pm 0.14	0.036	1.04	3.38	-
111 Cd	0.17 \pm 0.01	3.35 \pm 0.06	1.07 \pm 0.02	6.78 \pm 0.07	0.146	3.17	1.045	-
120 Sn	1.81 \pm 0.06	34.8 \pm 0.7	99.6 \pm 1.4	40.7 \pm 0.7	2.77	32.5	195	-
121 Sb	0.32 \pm 0.01	11.5 \pm 0.3	2.00 \pm 0.06	7.53 \pm 0.13	0.37	12.5	2.78	-
133 Cs	2.04 \pm 0.05	1.02 \pm 0.01	31.4 \pm 0.4	3.65 \pm 0.02	1.89	1.07	30.6	-
139 La	17.3 \pm 0.4	10.6 \pm 0.1	19 \pm 0.2	15.9 \pm 0.2	18.1	11.3	19.8	16
140 Ce	34.1 \pm 1.1	21.9 \pm 0.4	41.9 \pm 0.5	32.4 \pm 0.3	34.4	23.4	42	-
141 Pr	4.39 \pm 0.15	2.93 \pm 0.03	4.46 \pm 0.08	3.86 \pm 0.03	4.05	2.4	3.09	-
146 Nd	17.4 \pm 0.4	12.2 \pm 0.2	16.5 \pm 0.3	15.1 \pm 0.1	17.6	13.2	15.7	-
147 Sm	3.66 \pm 0.07	2.84 \pm 0.1	3.26 \pm 0.04	3.31 \pm 0.06	3.48	2.68	3.26	-
151 Eu	0.97 \pm 0.01	0.84 \pm 0.02	0.64 \pm 0.01	0.84 \pm 0.03	0.925	0.81	0.686	-
157 Gd	3.18 \pm 0.07	2.83 \pm 0.06	2.61 \pm 0.09	3.14 \pm 0.05	2.71	2.67	2.63	-
159 Tb	0.46 \pm 0.01	0.45 \pm 0.01	0.37 \pm 0.01	0.50 \pm 0.01	0.431	0.44	0.368	-
163 Dy	2.62 \pm 0.06	2.75 \pm 0.09	2.11 \pm 0.02	3.01 \pm 0.02	2.23	2.86	2.22	-
165 Ho	0.49 \pm 0.03	0.56 \pm 0.01	0.39 \pm 0.005	0.60 \pm 0.01	0.318	0.678	0.443	-
167 Er	1.37 \pm 0.06	1.59 \pm 0.03	1.11 \pm 0.05	1.79 \pm 0.03	0.906	1.48	1.07	-
169 Tm	0.19 \pm 0.01	0.21 \pm 0.01	0.15 \pm 0.01	0.25 \pm 0.01	0.13	0.23	0.155	-
173 Yb	1.23 \pm 0.05	1.44 \pm 0.02	1.05 \pm 0.03	1.66 \pm 0.04	1.18	1.67	1.4	-
175 Lu	0.18 \pm 0.01	0.19 \pm 0.01	0.16 \pm 0.01	0.25 \pm 0.01	0.186	0.252	0.196	-
178 Hf	0.73 \pm 0.03	0.82 \pm 0.02	1.16 \pm 0.04	2.01 \pm 0.09	3.55	2.7	3.21	-
181 Ta	0.90 \pm 0.02	0.37 \pm 0.01	0.56 \pm 0.016	0.76 \pm 0.01	0.893	0.515	0.687	-
205 Tl	0.37 \pm 0.01	0.46 \pm 0.02	2.21 \pm 0.06	0.85 \pm 0.02	0.407	0.45	2.06	-
Pb ^a	14.3 \pm 0.3	155 \pm 2	86.5 \pm 1.6	243 \pm 3	12.9	146	82.1	240
209 Bi	0.11 \pm 0.01	1.07 \pm 0.01	15.4 \pm 0.2	5.61 \pm 0.02	0.106	1.36	12.8	-
232 Th	4.47 \pm 0.11	2.30 \pm 0.02	6.90 \pm 0.10	4.94 \pm 0.06	4.44	2.33	7.79	-
238 U	0.89 \pm 0.01	0.91 \pm 0.01	1.28 \pm 0.02	2.37 \pm 0.02	1	1.1	1.66	-

^a Sum of ²⁰⁶Pb, ²⁰⁷Pb, and ²⁰⁸Pb^b The reference values are from Imai *et al.* (1996), Terashima *et al.* (2002), and the certificate for JSd-4.

we optimized the operation parameters for the ISIS3 to efficiently measure a large number of samples. Compared to the previous ISIS system, the ISIS3 was shortened the time duration of a single measurement of a sample, which includes loading, sample dilution, signal stabilization, and washing, by approximately 100 s. For the multi-element analysis of the geochemical samples, we employed a matrix-matched standard solution. The standard solution was a JB-1a-based solution with added Li, Be, Ni, Cu, Zn, As, Mo, Ag, Cd, Sn, Sb, Cs, Tl, Pb, and Bi. The concentrations of 42 elements in geochemical reference materials measured using the newly setup ICP-MS were comparable to their recommended/referenced values, indicating that the experimental setup for multi-element and large amount of sample analyses was satisfactory.

Acknowledgements

This work was supported by a grant from the GSJ. We would like to thank Tachibana, Y. for their assistance. We would like to thank an anonymous reviewer and Editor Togo, Y. for their helpful comments.

References

- Douglas, D. J. and French, J. B. (1992) Collisional focusing effects in radio frequency quadrupoles. *Journal of the American Society for Mass Spectrometry*, **3**, 398–408.
- Imai, N. (1990) Multielement analysis of rocks with the use of geological certified reference material by inductively coupled plasma mass spectrometry. *Analytical Sciences*, **6**, 389–395.
- Imai, N., Terashima, S., Itoh, S. and Ando, A. (1995) 1994 compilation of analytical data for minor and trace-elements in 17 GSJ geochemical reference samples, igneous rock series. *Geostandards Newsletter*, **19**, 135–213.
- Imai, N., Terashima, S., Itoh, S. and Ando, A. (1996) 1996 compilation of analytical data on nine GSJ geochemical reference samples, “Sedimentary rock series”. *Geostandards Newsletter*, **20**, 165–216.
- Imai, N., Terashima, S., Ohta, A., Mikoshihara, M., Okai, T., Tachibana, Y., Togashi, S., Matsuhisa, Y., Kanai, Y., Kamioka, H. and Taniguchi, M. (2004) *Geochemical map of Japan*. Geological Survey of Japan, AIST.
- Imai, N., Terashima, S., Ohta, A., Mikoshihara, M., Okai, T., Tachibana, Y., Togashi, S., Matsuhisa, Y., Kanai, Y. and Kamioka, H. (2010) *Geochemical Map of Sea and Land of Japan*. Geological Survey of Japan, AIST.
- Imai, N., Okai, T., Ohta, A., Mikoshihara (Ujiie), M., Kanai, Y., Kubota, R., Tachibana, Y., Terashima, S., Ikehara, K., Katayama, H. and Noda, A. (2015) *Geochemical Map of Kanto Region*. Geological Survey of Japan, AIST.
- Imai, N., Okai, T., Ohta, A., Mikoshihara (Ujiie), M., Kubota, R., Atsunori N., Tachibana, Y., Terashima, S., Ikehara, K., Katayama, H. and Noda, A. (2019) *Geochemical Map of the Chubu Region*. Geological Survey of Japan, AIST.
- McCurdy, E., Woods, G. and Potter, D. (2006) Unmatched removal of spectral interferences in ICP-MS Using the Agilent Octopole Reaction System with helium collision mode. Application, Agilent Technologies, Inc., Santa Clara, 1–7. <https://www.agilent.com/cs/library/applications/5989-4905EN.pdf> (Accessed: 2022-12-02)
- Nakamura, A., Okai, T. and Ohta, A. (2020) Optimizing the Pratt-type titrimetric method to determine FeO in geochemical reference materials. *Geochemical Journal*, **54**, 337–350.
- Nakamura, A., Ohta, A., Matsuzaki, H. and Okai, T. (2021) $^{10}\text{Be}/^{9}\text{Be}$ ratios of phenakite and beryl measured via direct Cs sputtering: Implications for selecting suitable Be carrier minerals for the measurement of low-level ^{10}Be . *Geochemical Journal*, **55**, 209–222.
- Ohta, A. (2018a) Evaluation of straightforward and rapid multi-element analyses of stream sediments for geochemical mapping in the remote islands of Japan — Seto Inland Sea region —. *Bulletin of the Geological Survey of Japan*, **69**, 1–30.
- Ohta, A. (2018b) Geochemical mapping of remote islands around Kyushu, Japan. *Bulletin of the Geological Survey of Japan*, **69**, 233–263.
- Ohta, A., Imai, N., Okai, T., Manaka, M., Kubota, R., Nakamura, A. and Tachibana, Y. (2021) Watershed analysis for geochemical mapping in Japan based on a hydrologic model: The concentrations of 53 elements and the dominant lithology in a drainage basin. *Geochemical Journal*, **55**, 59–88.
- Okai, T. (2016) Development and utilization of geochemical reference materials—Reliability improvement in the analysis of geological materials—. *Synthesiology English edition*, **9**, 60–73.
- Proper, W., McCurdy, E. and Takahashi, J. (2020) Performance of the Agilent 7900 ICP-MS with UHMI for High Salt Matrix Analysis. Application Note, Agilent Technologies, Inc., Santa Clara, 1–9. https://www.agilent.com/cs/library/applications/5991-4257EN_AppNote7900_ICP-MS_salt.pdf (Accessed: 2022-12-02)
- Takahashi, J. and Yamada, N. (2004) Development of collision/reaction cell for reduction of spectral interference in ICP mass spectrometry. *Bunseki Kagaku*, **53**, 1257–1277.
- Tanner, S. D., Baranov, V. I. and Bandura, D. R. (2002) Reaction cells and collision cells for ICP-MS: a tutorial review. *Spectrochimica Acta Part B: Atomic Spectroscopy*, **57**, 1361–1452.
- Terashima, S. (2001) Determination of indium and tellurium in fifty nine geological reference materials by solvent extraction and graphite furnace atomic absorption spectrometry. *Geostandards Newsletter*, **25**, 127–132.
- Terashima, S., Imai, N., Taniguchi, M., Okai, T. and Nishimura, A. (2002) The preparation and preliminary

- characterisation of four new Geological Survey of Japan geochemical reference materials: Soils, JSO-1 and JSO-2; and marine sediments, JMS-1 and JMS-2. *Geostandards Newsletter*, **26**, 85–94.
- Wilbur, S. and Jones, C. (2010) Maximizing productivity in high matrix samples using the Agilent 7700x ICP-MS with ISIS discrete sampling. Application Note, Agilent Technologies, Inc., Santa Clara, 1–9. <https://www.agilent.com/cs/library/applications/5990-5437EN.pdf> (Accessed: 2022-12-02)
- Yamanaka, K. and Wilbur, S. (2014) Maximizing productivity for high matrix sample analysis using the Agilent 7900 ICP-MS with ISIS 3 discrete sampling system. Application note, Agilent Technologies, Inc., Santa Clara, 1–12. https://www.agilent.com/cs/library/applications/5991-5208EN_AppNote7900_ICP-MS_soil.pdf (Accessed: 2022-12-02)
- Received July 15, 2022
Accepted December 6, 2022

インテグレートサンプル導入システムとガス希釈システムを搭載した ICP-MS による 高マトリックス地質試料の多元素分析

中村 淳路・久保田 蘭・太田 充恒

要 旨

誘導結合プラズマ質量分析器(ICP-MS)の発展により、さまざまな地質試料の多元素分析が行われるようになってきた。しかし、高マトリックス試料を効率的に迅速に分析することは依然として困難を伴っている。そこで本研究は、高マトリックス地質試料の迅速分析を目的として新たに導入したAgilent 7900 ICP-MSのパフォーマンスと、各種設定値の調整結果を報告する。ICP-MSにはコリジョン/リアクションセル(CRC)、ガス希釈による高マトリックス試料導入(UHMI)システム、第三世代のインテグレートサンプル導入システム(ISIS3)を搭載した。まず、CRCによる効果的な分子干渉の抑制を目指して、Heガス流量の最適化を行った。その結果、4.5 mL/minのHeガス流量において、最適なバックグラウンド相当濃度およびブランク/標準試料比を得ることができた。UHMIシステムはマトリックス効果を抑制し、さらに二価イオン、酸化物イオン、プラズマ由来の分子イオン、酸由来の分子イオン、マトリックス由来の分子イオンによる干渉抑制にも効果を発揮する。本研究ではHMI-8モード(10倍希釈)を用いた時の効果を検討し、UHMIシステムが酸化物イオンとマトリックス由来の分子イオンの抑制に特に効果的であることを確認した。なお、高マトリックスの地質試料に対しては、内標準によるマトリックス効果の補正は有効でない。そこで本研究はマトリックスマッチング法を適用した。地球化学標準物質JB-1aを元とする溶液に、Li, Be, Ni, Cu, Zn, As, Mo, Ag, Cd, Sn, Sb, Cs, Tl, Pb, Biを添加することで、標準液を調製した。ISIS3を用いたルーチン分析として50試料中の42元素を測定した場合、従来の水希釈による試料導入装置と比較し、測定時間を約80分短縮することができた。ICP-MS本体およびその周辺装置について各種設定値を最適化し、8つの地球化学標準物質中の42元素の測定を行った結果、参照値と同等の測定値が得られることを確認した。

